buildings

MDPI

Article

Analysis of Flexural Performance and Crack Width Prediction Models of UHPC Composite Slabs

Chao Liu [1,2], Yuexia Li [3,*], Jiwang Zhang [1,2,*] and Dongwei Wan [4]

[1] Guangxi Key Laboratory of Green Building Materials and Construction Industrialization, Guilin University of Technology, Guilin 541004, China
[2] School of Civil Engineering, Guilin University of Technology, Guilin 541004, China
[3] Nanning College of Technology, Guilin 541006, China
[4] Guilin University of Electronic Technology, Guilin 541004, China
* Correspondence: liyuexia@nnct.edu.cn (Y.L.); 2020131@glut.edu.cn (J.Z.)

Abstract

To study the crack resistance of UHPC precast composite slabs, this paper conducts flexural performance tests on one UHPC monolithic slab and four UHPC precast composite slabs, investigating the influence of structural form, loading method, and shear reinforcement on the failure mode and crack resistance of UHPC precast composite slabs. The test results showed that UHPC precast composite slabs do not experience shear failure along the composite interface. They exhibit extensive microcracks and do not fail due to the immediate appearance of a single wide crack, demonstrating good plasticity and toughness. The cracking load of the monolithic slab is 6.6% to 12.5% higher than that of the composite slabs. However, the yield load and ultimate load of composite slabs equipped with shear reinforcement are 19.5% to 26.5% and 24.5% to 29.5% higher than those of the monolithic slab, respectively. These composite slabs are also characterized by extensive, dense microcracks with high quantity, small width, small spacing, short length, and dense distribution. Shear reinforcement can effectively improve the bearing capacity and crack resistance of UHPC precast composite slabs, with truss reinforcement showing a better effect in enhancing bearing capacity and inhibiting cracks. The comparison between positive and reverse loading methods better explains the "strain lag" of concrete and "stress advance" of reinforcement in composite slabs. Based on the section internal force equilibrium and the bond stress transfer principle between reinforcement and concrete, considering the enhancement effect of UHPC on bond stress, the calculation formulas for average crack spacing and maximum crack width in existing codes are modified. The calculated values are in good agreement with the test results.

Keywords: ultra-high performance concrete; composite slabs; crack resistance performance; crack width

Check for updates

Academic Editors: Mu-Xuan Tao and Li-Yan Xu

Received: 19 December 2025
Revised: 13 January 2026
Accepted: 15 January 2026
Published: 19 January 2026

Copyright: © 2026 by the authors. Licensee MDPI, Basel, Switzerland. This article is an open access article distributed under the terms and conditions of the Creative Commons Attribution (CC BY) license.

1. Introduction

Ultra-high performance concrete (UHPC) is a cement-based composite material with extremely high strength, high toughness, high durability and excellent impermeability [1–3]. It overcomes the problems of easy cracking and brittleness of traditional concrete and has been increasingly widely used in recent years [4]. UHPC prefabricated composite slab is an innovative component [5,6] that uses UHPC as the precast layer and connects the cast-in-place concrete through shear reinforcement on the composite interface. It can meet

the requirements of modern buildings for large space, long span, and convenient construction, and promote the development of major infrastructure such as modern super high-rises, bridges, offshore platforms, and nuclear power plants towards lightweight, high performance and high durability [7,8]. However, with the wide application of prefabricated building projects, the insufficient cooperative working performance of concrete at the composite interface of composite components leads to frequent cracking of composite components, which seriously affects the mechanical performance and normal service function of the structure. This problem has attracted increasing attention from the engineering community [9,10].

To investigate the mechanical performance of UHPC composite slabs, experts and scholars in China and globally have conducted a series of experimental studies and theoretical analyses on the performance of composite slabs [11–13]. Shiming Chen et al. [14] carried out finite element analysis on the bearing capacity of composite slabs based on the interface contact model, providing strong support for the design and application of composite slabs. The connecting reinforcement of composite slabs can effectively share the tensile stress of longitudinal reinforcement during loading, significantly improving the bearing capacity and flexural stiffness of the components [15–17]. Ren Y et al. [18] used finite element software (Abaqus) to analyze the concrete plastic damage mechanism, studied the failure mode of closely joined composite slabs under loading, and pointed out that the current design principle of two-way slabs can be applied to the design and calculation of closely joined slabs. Thanoon [19] proposed that truss reinforcement, as shear connectors embedded in precast concrete slabs, can ensure good integrity of composite slabs at all stages of bending. Bin Luo et al. [20,21] investigated the differences in the flexural performance of composite concrete slabs with varied structural configurations, analyzed the influence mechanism governing the flexural stiffness of composite slabs, and proposed a calculation formula for their short-term stiffness. Rahman MK [22,23] conducted experimental studies on steel truss concrete hollow composite slabs of different sizes and thicknesses. The results showed that no horizontal cracks propagated along the composite interface of the composite slabs, the precast layer and cast-in-place layer had good cooperative working performance, the cracks at the bottom of the slabs were evenly distributed, and the overall deformation performance was excellent. Kaozhong Zhao [24] proposed that the high-strength concrete composite slab formed by combining high-strength concrete and steel trusses is a new type of load-bearing system with high comprehensive benefits. Zhuangcheng Fang et al. [25] developed a steel–concrete composite slab beam based on a new type of hybrid fiber material, which can improve the crack resistance of the component and proposed a calculation formula for the flexural crack width of the component.

However, for the new-type material UHPC, research on structural design is relatively weak, and research on composite components is even more scarce. At present, the accumulation of experimental data on the crack resistance of UHPC composite components is insufficient, and a complete set of calculation formulas for crack resistance suitable for UHPC composite components has not yet been established [26]. This undoubtedly brings certain challenges and limitations to the application of UHPC in practical engineering.

Combining the advantages of existing concrete composite slabs, this research investigates the effects of structural forms, shear reinforcement, and loading methods on the crack resistance of UHPC composite slabs. It focuses on analyzing the failure modes, crack width and distribution, crack resistance mechanism, and crack calculation of UHPC specimens, aiming to provide references for practical engineering applications. The research addresses problems of traditional composite slabs such as insufficient crack resistance, low bearing capacity, and poor durability, and has important engineering significance for

promoting the application of UHPC composite slabs in fields like bridges, tunnels, and marine engineering.

2. Materials and Experimental Methods

2.1. Materials

Table 1 summarizes the mix proportions of the UHPC. The raw materials of UHPC consist of P.O 42.5 Portland cement, silica fume, silica powder, fly ash, and quartz sand, supplemented with a superplasticizer and steel fibers [27]. Among these materials, silica fume has a particle size of 0.1–0.2 μm and an SiO_2 content of over 94.7%, with its morphology illustrated in Figure 1a. The quartz sand, with a SiO_2 content exceeding 99.6%, exhibits spherical particles, a continuous and well-graded distribution, and an average particle size ranging from 0.4 to 0.6 mm, as illustrated in Figure 1b. Silica powder has an average particle size of 0.1 μm and exhibits excellent pozzolanic activity, as illustrated in Figure 1c. Fly ash is spherical in shape, with a particle size of less than 100 μm. The chemical compositions of the cementitious materials are shown in Table 2. Additionally, a polycarboxylate-based high-efficiency superplasticizer with a 25% water reduction rate from Beijing Oriental Yida Building Materials Co., Ltd. (Beijing, China). is incorporated. The steel fibers are thin, round, and copper-plated on the surface, with a diameter of 0.22 mm, a length of 12 mm, and an aspect ratio of 55. Tap water is used as the mixing water.

Table 1. Mixture proportions of UHPC (mass ratio relative to cement).

Cement	Quartz Sand	Silica Fume	Silica Powder	Fly Ash	Water	Steel Fiber (Volume Fraction)/%	Water-Reducer
1	1.2	0.15	0.05	0.1	0.23	2	0.02



(**a**) (**b**) (**c**)

Figure 1. Raw materials: (**a**) silica fume, (**b**) quartz sand, and (**c**) silica powder.

Table 2. Chemical analysis of the used cementitious materials (%).

Materials	CaO	SiO_2	MgO	Al_2O_3	P_2O_5	Na_2O	SO_3	K_2O	Fe_2O_3
Cement	60.15	23.19	0.88	7.08	0.13	0.14	3.01	0.61	3.62
Silica powder	0.13	96.47	0.02	0.15	0.13	-	-	-	0.13
Fly ash	4.48	55.34	1.86	22.42	0.78	1.67	1.34	2.21	8.51
Silica fume	0.34	94.7	0.49	0.26	0.18	0.15	0.71	0.82	0.17

The mechanical properties of ultra-high performance concrete (UHPC) were evaluated based on the specimens prepared in accordance with References [4,5] and the national Standard for Test Methods of Mechanical Properties on Ordinary Concrete. Specifically, 100 mm × 100 mm × 100 mm cubic specimens were utilized for both cube compressive strength and splitting tensile strength tests, whereas φ100 mm × 200 mm cylindrical specimens were adopted to assess axial compressive strength. For steel reinforcement, its mechanical properties were tested following the Standard Test Methods for Tensile Testing

of Metallic Materials at Room Temperature to determine the yield strength and ultimate tensile strength. Detailed results of all mechanical property tests for both UHPC and steel reinforcement are presented in Tables 3 and 4.

Table 3. Mechanical properties of UHPC.

Material	Elastic Modulus (GPa)	Cube Compressive Strength (MPa)	Axial Compressive Strength (MPa)	Splitting Tensile Strength (MPa)
UHPC	42	139.5	118	8.2

Table 4. Mechanical properties of steel reinforcements.

Diameter (mm)	Elastic Modulus (GPa)	Yield Strength (MPa)	Tensile Strength (MPa)
Φ12	201	435	556
Φ10	203	481	638
Φ8	205	468	560
Φ6	206	478	637

2.2. Specimen Design

Based on the results of previous research [27], the casting quality of the composite slab is relatively stable. Accordingly, five UHPC test slabs were designed and fabricated for the experiment, including four UHPC composite slabs and one monolithic UHPC slab serving as a control specimen. For Specimen DB-1, the variable is the volume ratio of shear reinforcement; for DB-2 and DB-3, the variable is the reinforcement detailing; and for DB-4, the variable is the loading surface of the slab. All test slabs have a dimension of 3020 mm × 600 mm × 130 mm. For the composite slabs, the thickness of the precast base slab is 70 mm, and the thickness of the cast-in-place layer is 60 mm. The distribution reinforcement at the bottom of both layers has a diameter of 8 mm and a spacing of 200 mm, while the tensile reinforcement has a diameter of 12 mm and a spacing of 150 mm. The cross-sectional configuration of the test slabs is shown in Figure 2, and detailed specimen parameters are presented in Table 5. A rough surface should be provided at the interface between the precast slab and the cast-in-place concrete, which is treated by artificial roughening. The area of the rough surface shall not be less than 80% of the interface area, and the concavo-convex depth of the rough surface shall not be less than 4 mm. Accordingly, we used handheld drilling equipment to chisel a 4 mm-deep uneven roughened surface across the entire casting interface.

Table 5. Main design parameters of test board.

Specimen Number	Length (*l*/mm)	Width (*b*/mm)	Thickness (*h*/mm)	Structural Form	Composite Surface Shear Steel Bars	Volume Reinforcement Ratio of Shear Resistant Steel Bars (ρ_v/%)	Loading Method
XB-1	3020	600	130	monolithic method	/	/	reverse
DB-1	3020	600	130	composite method	/	0	reverse
DB-2	3020	600	130	composite method	stirrup stool	0.4	reverse
DB-3	3020	600	130	composite method	truss reinforcement	0.4	reverse
DB-4	3020	600	130	composite method	truss reinforcement	0.4	forward

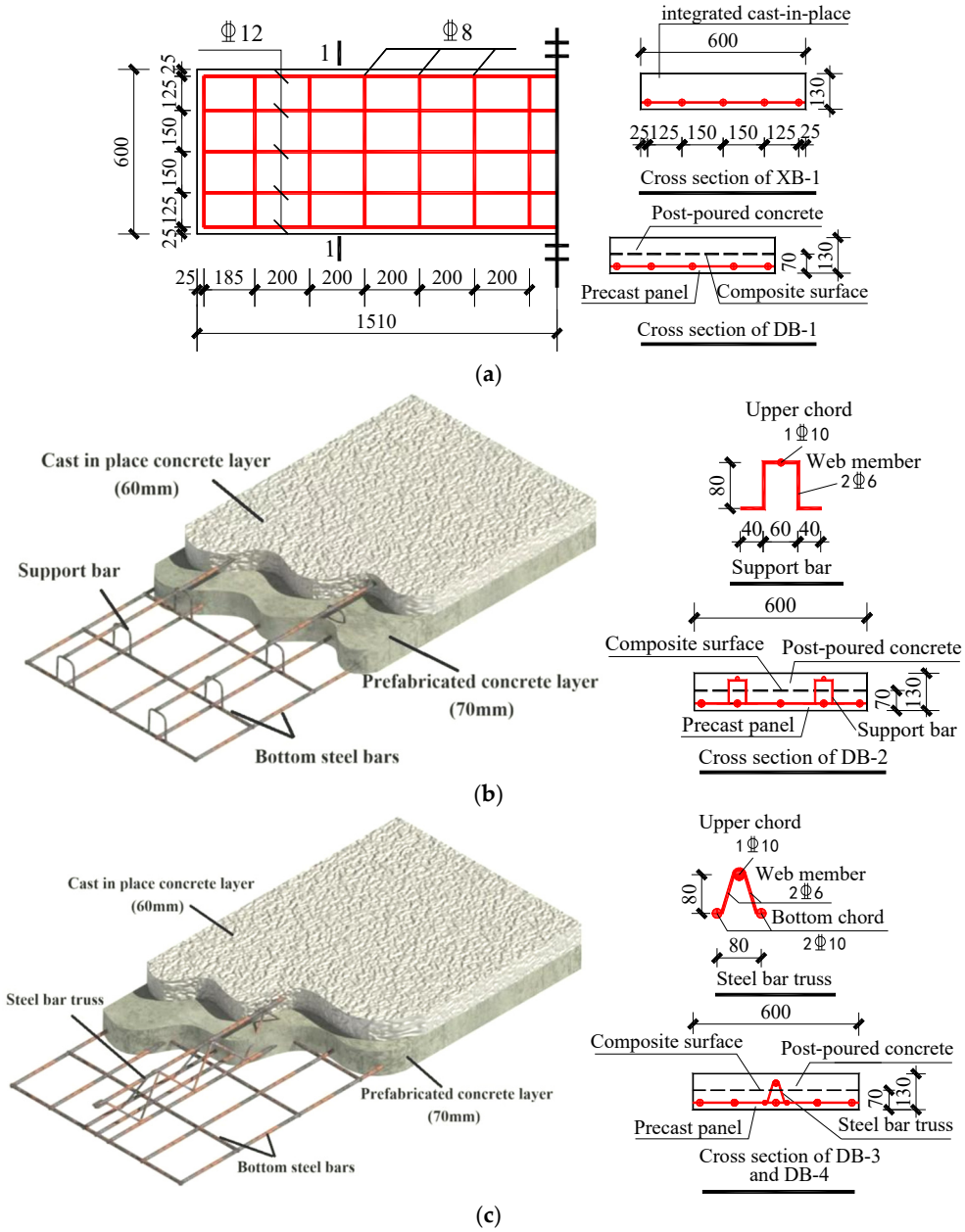
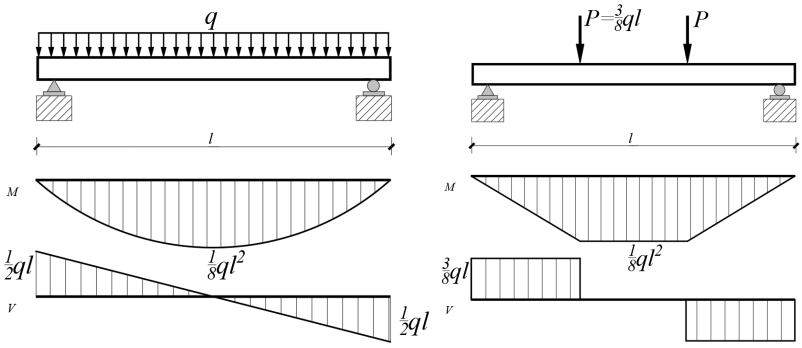


Figure 2. Dimensions and reinforcement diagram of the test plate. (**a**) Section construction and reinforcement of integral cast slab and non-shear reinforced composite slab. (**b**) Sectional structure and reinforcement of horse stool-reinforced concrete composite panel. (**c**) Section construction and reinforcement of truss-reinforced concrete composite panel.

2.3. Loading Scheme

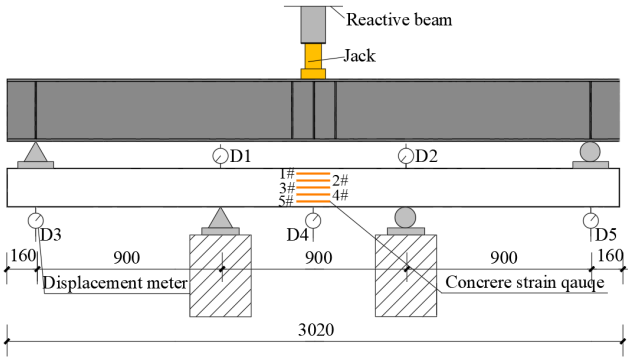
There are generally two loading methods in static loading tests. The first is the uniform load method, where load blocks are stacked uniformly in zones to simulate uniform loading, and the force condition is shown in Figure 3a. The second is the equivalent load method, which adopts three-point loading to equate two concentrated loads to a uniform load [11]. Restricted by test conditions, the uniform load method is difficult to implement, so the equivalent load method was adopted in this test. The equivalent load method uses a jack and distribution beam system to simulate uniform loading. This method ensures that when the bending moment at the mid-span section of the slab during the test is equal to that under uniform loading, the maximum shear force at the supports is approximately equal to that under uniform loading. The schematic diagram of the equivalent load method is shown in Figure 3b.



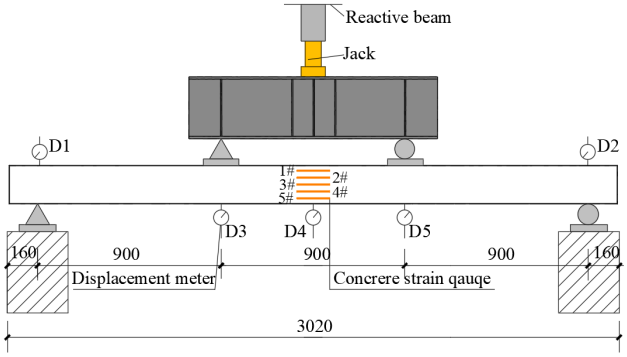
(**a**) Uniform load method (**b**) Equivalent load method

Figure 3. Load loading diagram.

The loading device is shown in Figure 4. The flexural test of the test slabs was conducted using a reverse step-by-step loading method with equivalent load via a jack and distribution beam system [13]. The test slabs were placed upside down on the supports to facilitate the observation of crack propagation and failure modes at the slab bottom. Among them, the test results of DB-4 under forward loading were calibrated by comparison with those of DB-3 under reverse loading. For the loading process: the loading was performed in stages. Before the crack width reached the limit value of 0.3 mm (serviceability limit state), the load applied at each stage did not exceed 20% of the design service load. When cracks were imminent, the load increment shall be refined, with loading implemented at 10% of the calculated ultimate load. When the crack width approached 1.5 mm (the allowable limit for the ultimate bearing capacity state), loading was continued at 10% of the calculated ultimate load until the member failed. After each load step is applied, the load shall be maintained for 10 min. After the load holding period, a flashlight and a magnifying glass were used to carefully observe the occurrence and development of cracks, and a crack width meter was employed to measure the crack width.



(**a**) Reverse loading



(**b**) Forward loading

Figure 4. Loading device diagram.

3. Test Results and Analysis

3.1. Failure Modes and Crack Characteristics

The failure modes and crack distributions of each test slab are shown in Figure 5. During the loading process of the specimens, the basic law of crack propagation is that cracks develop slowly from the third-point positions at the slab bottom toward the mid-span of the slab bottom; most cracks are concentrated in the pure bending zone, with their direction parallel to the slab width direction. When the crack width exceeds the 0.3 mm limit for normal service condition specified, the growth of the main crack width accelerates, the test slab exhibits bending deformation, and a squeaking sound (from steel fibers being pulled out) can be heard. At failure, no delamination is observed at the composite interface, and no shear failure occurs along the composite interface. The composite slab maintains good integrity at all stages of bending. All specimens show consistent failure modes: the crack width reaches the 1.5 mm failure criterion specified, with obvious bending behavior and good plastic performance, which are characteristics of ductile failure.

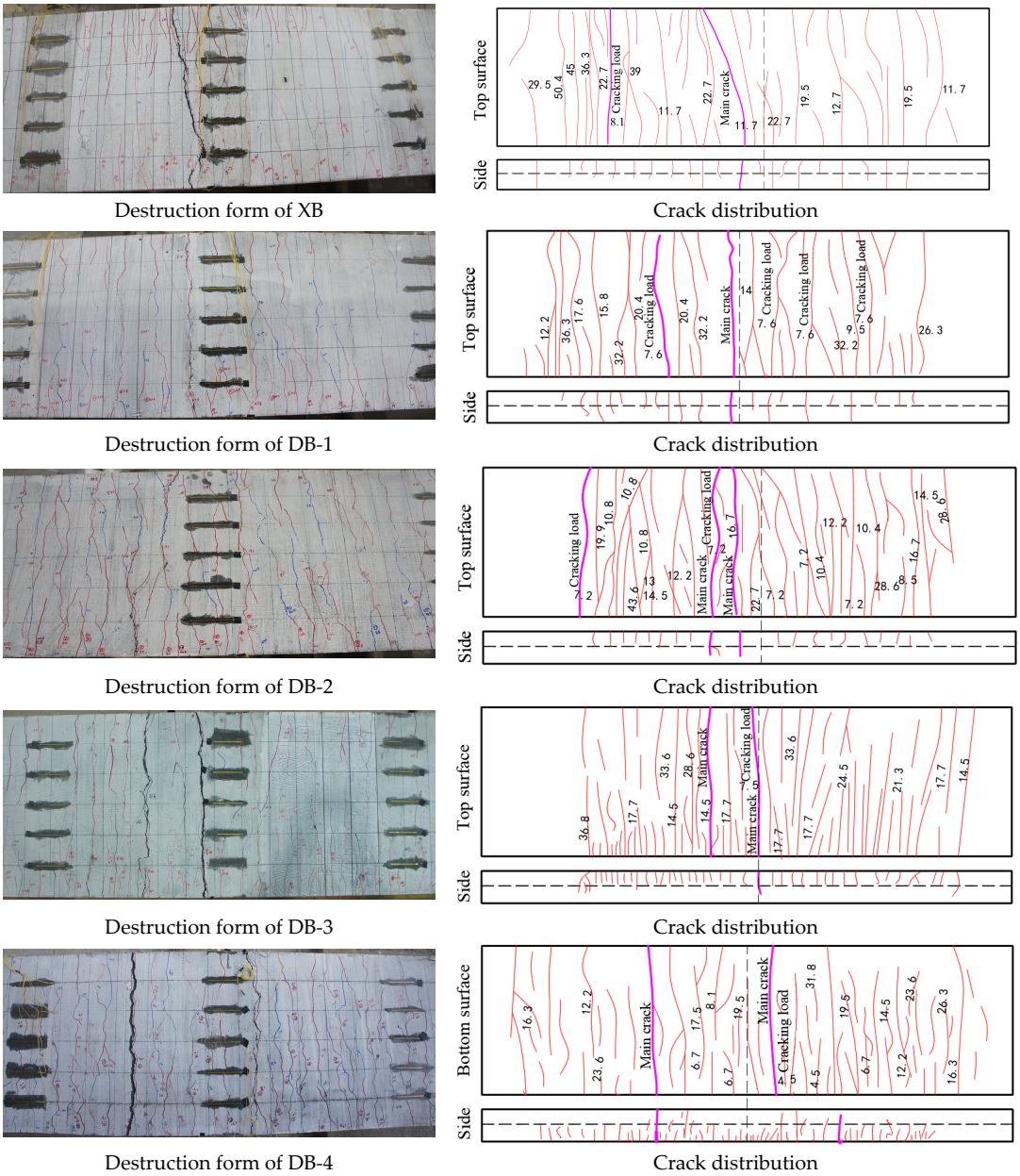


Figure 5. Failure modes and crack distribution of composite reinforced concrete slabs.

The distribution of crack width proportion in test slabs is shown in Figure 6. Cracks with a width greater than 0.3 mm are few in number but highly harmful; some of them have penetrated the slab bottom and even extended to the composite interface, forming main cracks. A certain number of cracks with a width of 0.1–0.2 mm are distributed on the slab surface or mid-span area. Microcracks with a width less than 0.1 mm account for a large proportion in all test slabs, exhibiting good plasticity at failure. As compared in Figure 5, the monolithic slab and composite slab DB-1 (without shear reinforcement) show little difference in crack quantity and width distribution. However, DB-2 to DB-4 with additional shear reinforcement have an increased number of cracks, and most of these cracks have a width less than 0.1 mm. A large number of fine cracks appear on the slab surface, distributing extensively in reticular or craquelure patterns. This indicates that shear key reinforcement can significantly improve the crack resistance and ductility of composite slabs, and truss reinforcement has a more obvious effect on enhancing their crack resistance and ductility. Cracks in such cases are characterized by a large quantity, small width, small spacing, short length, and dense distribution.

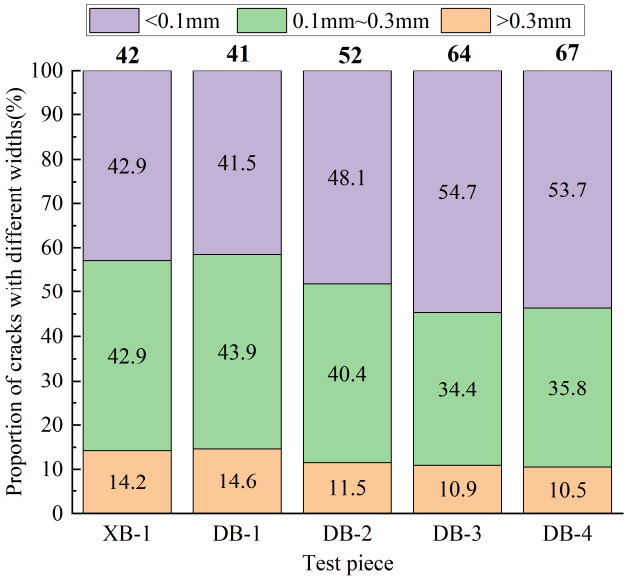


Figure 6. Distribution of the proportion of crack width quantity.

3.2. Load-Deflection Analysis

The deflection curves of specimens XB-1 and DB-1 to DB-4 can be categorized into the following three distinct stages: the elastic stage prior to cracking of the concrete, the elastoplastic stage subsequent to cracking, and the unloading descending phase following failure, as illustrated in Figure 7. Before the cracking of the concrete, a linear relationship existed between load and mid-span displacement for all specimens, confirming their elastic bending behavior. After cracking occurred, the slope of the load-deflection curves gradually decreased. With increasing load, the reinforcing bars yielded sequentially, resulting in an accelerated deflection growth rate and indicating the transition of the specimens into the elastoplastic working stage. Following the formation of main cracks, both deflection and crack width developed rapidly, with measured maximum deflections of 35.82 mm, 36.09 mm, 35.54 mm, 44.09 mm, and 45.2 mm, respectively. After unloading, the cracks exhibited good closure performance, and the deflection curves displayed a plump profile. The mid-span residual displacements of the specimens were 18.52 mm, 20.69 mm, 17.03 mm, 19.9 mm, and 19.4 mm, respectively, corresponding to deflection recovery rates of 43–57% These results demonstrate that the UHPC specimens possess favorable elastic recovery capacity.

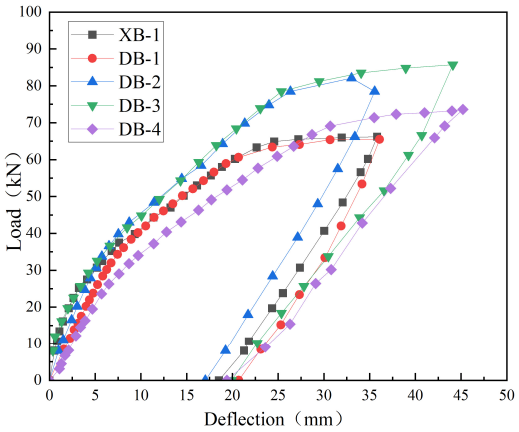


Figure 7. Load-deflection curve.

3.3. Crack Resistance Capacity Analysis

The cracking load F_{cr}, the load $F_{0.3}$ corresponding to a crack width of 0.3 mm, and the ultimate load F_u recorded in the test are presented in Table 6. Under the same reverse loading condition, the cracking load of the monolithic slab is 6.6%, 12.5%, and 8% higher than that of the composite slabs without shear reinforcement, with stirrup stools, and with truss reinforcement, respectively. This is because composite slabs have inherent weak points formed before concrete hardening—points that do not exist in monolithic slabs—leading to differences in their crack resistance performance. The cracking loads of composite slabs DB-1 to DB-3 show little difference, indicating that shear reinforcement has minimal impact on the cracking load. After cracking, as the load increases, differences in the load-bearing capacity of the specimens gradually become apparent.

Table 6. Load index of test piece.

Load (kN)	Test Piece				
	XB-1	**DB-1**	**DB-2**	**DB-3**	**DB-4**
F_{cr}	8.1	7.6	7.2	7.5	4.5
$F_{0.3}$	58.4	58.9	69.8	73.9	68.9
F_u	66.2	65.5	82.1	85.7	73.6

The yield load of composite slabs with stirrup stools and truss reinforcement is 19.5% and 26.5% higher than that of the monolithic slab, and 18.5% and 26.5% higher than that of the composite slab without shear reinforcement, respectively. Their ultimate load is 24% and 29.5% higher than that of the monolithic slab, and 25.3% and 30.8% higher than that of the composite slab without shear reinforcement, respectively. This is because the shear reinforcement arranged at the composite interface can increase the height of the neutral axis and the effective cross-sectional height, thereby enhancing deformation resistance and load-bearing capacity. Among them, truss reinforcement has a better effect in improving structural stiffness, deformation resistance, and crack resistance: its web members penetrate the composite interface, acting like numerous "pins" to firmly lock the precast layer and cast-in-place layer together. This enhances the member's integrity and cross-sectional stiffness, significantly improving the crack resistance of the precast base slab. In addition, the two bottom chords of the truss reinforcement directly strengthen the constraint on the concrete in the tensile zone—exerting a more significant effect than the top chords of stirrup stools (which bear small compressive stress before cracking). The improvements in serviceability limit load and ultimate bearing capacity are also quite obvious.

A comparative analysis of DB-3 and DB-4 (with different loading methods) shows differences in the cracking load and ultimate load of composite slabs under forward and reverse loading. Under reverse loading, all observed values of DB-3 are higher than those under forward loading. This is because under reverse loading, the slab bottom faces upward: the bending moment it bears is not affected by self-weight; instead, self-weight offsets part of the bending moment, resulting in larger bending moment values for the composite slab under reverse loading.

3.4. Crack Width Analysis

The load-main crack width curves of the test slabs are shown in Figure 8. The curve changes in the composite slab without shear reinforcement (DB-1) are quite similar to those of the monolithic slab (XB-1). After the appearance of diagonal cracks, the change in curve slope takes around 40 kN as the dividing point. Before this dividing point, the curves of all test slabs basically coincide, indicating that within a period after crack initiation, concrete gradually ceases to work, and the steel fibers spanning the cracks in UHPC begin to exert a "bridging effect" [28–30] to restrict crack development. After the dividing point, there are obvious differences in the slope of each curve. For specimens equipped with shear reinforcement (DB-2 to DB-4), their curvature decreases and the growth rate of crack width slows down, demonstrating that the inhibitory effect of shear reinforcement on cracks is significantly enhanced. Among them, composite slabs with truss reinforcement exhibit the optimal crack inhibition effect. When the load reaches around 57 kN, DB-1 shows a turning point earlier than XB-1, and the crack width rises linearly. The composite slab without shear reinforcement takes the lead in entering the stage of rapid crack width development, and the tensile reinforcement yields earlier than that of the monolithic slab—this is referred to as the "stress advancement" phenomenon of tensile reinforcement.

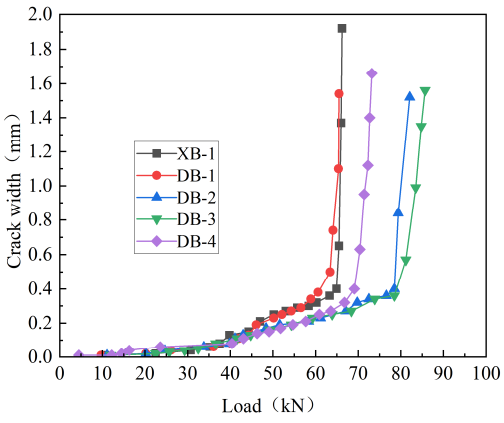


Figure 8. Load-crack width curve.

A comparison of DB-3 and DB-4 (both equipped with the same shear truss reinforcement but different loading methods) shows that under reverse loading, DB-3 first needs to offset the deformation caused by self-weight and undergoes a deflection reversal process. Thus, its cracking occurs later than that of DB-4 under forward loading. However, after cracking, the load-deformation curves of the two are roughly parallel, and their crack development patterns are basically consistent.

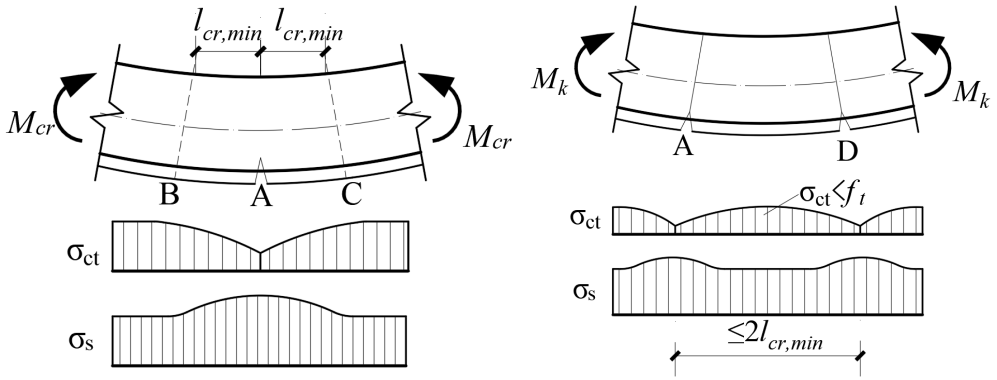
4. Analysis on Crack Width Calculation Model

4.1. Crack Resistance Mechanism Analysis

Under load action, the initiation and propagation of cracks in test slabs can be divided into the following two categories:

(1) Occurrence of the first batch of cracks:

When the flexural tensile stress induced by the load exceeds the tensile strength of concrete, one or several initial cracks first appear at the tensile edge of the weakest section at the mid-span of the slab bottom in the pure bending zone. The initiation of these cracks is random. After section cracking, concrete gradually ceases to work and shrinks toward both sides of the cracks, while the stress of the reinforcement at the cracked section increases by taking over the stress previously borne by concrete. However, due to the bridging and crack-inhibiting effect [31] of steel fibers in UHPC between the cracked concrete, the stress of concrete at the cracked area is not zero, as shown in Figure 9a.



(**a**) The first batch of cracks appeared (**b**) The second batch of cracks appeared

Figure 9. The appearance and development of cracks (σ_{ct}: concrete strain, σ_s: reinforcement strain).

(2) Occurrence of the second batch of cracks:

With the increase in load, at a certain distance, $l_{cr,\min}$, from the first batch of cracks (e.g., points B and C), the accumulation of bond stress between the reinforcement and concrete causes the concrete tensile stress to reach the tensile strength again, leading to the appearance of the second batch of cracks in the member. If the accumulation of bond stress is insufficient to make the concrete tensile stress reach its tensile strength ($\sigma_{ct} < f_t$), no new cracks will appear between existing cracks, as shown in Figure 9b. For the entire member, the crack spacing will eventually stabilize between $l_{cr,\min}$ and 2 $l_{cr,min}$, with the average crack spacing being approximately 1.5 $l_{cr,min}$.

4.2. Average Crack Spacing l_{cr}

The stress state of reinforcement and concrete between cracks is shown in Figure 10. Take a local free body for force balance analysis. Assuming the spacing between two cracks is l_{cr}, Equation (1) can be derived from the force balance equation. Then take the reinforcement as a free body. Assuming the average bond stress is τ_m and the total perimeter of the reinforcement is μ, the relational expression (2) can be obtained according to the balance condition. Combining Equations (1) and (2), the relationship between the average crack spacing, concrete cross-sectional area, and tensile strength of reinforcement is shown in Equation (3). At this time, the effective diameter of the tensile reinforcement is d_{eq}, with its effective area $A_S = \pi {d_{eq}}^2/4$ and perimeter $\mu = \pi d_{eq} = 4A_S/d_{eq}$. Through relational conversion, the average crack spacing can be obtained as shown in Equation (4):

$$A_s\sigma_{s1} - A_c f_t = A_s\sigma_{s2} \quad (1)$$

$$A_s\sigma_{s1} - A_s\sigma_{s2} = \tau_m u l_{cr} \quad (2)$$

$$\tau_m u l_{cr} = A_c f_t \quad (3)$$

$$l_{cr} = \frac{A_c f_t}{\tau_m} \cdot \frac{d_{eq}}{4A_s} = \frac{f_t}{4\tau_m} \cdot \frac{d_{eq}}{\rho_{eq}} \tag{4}$$

In the formula, A_C: cross-sectional area of concrete; A_S: effective cross-sectional area of the reinforcement; σ_S: reinforcement stress; and ρ_{eq}: effective reinforcement ratio, where $\rho_{eq} = A_S/A_C$.

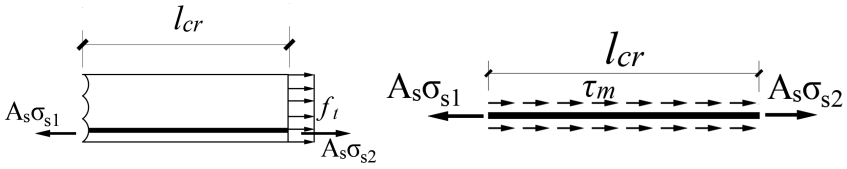


Figure 10. Schematic diagram of the stress state of steel bars and concrete between cracks.

Based on the bond force transfer principle, crack spacing is mainly related to the bond stress τ_m between reinforcement and concrete, as well as the area of tensile concrete. This is reflected in aspects such as reinforcement ratio, reinforcement diameter, concrete cover thickness, and surface characteristic coefficient of reinforcement. Scholars worldwide [32,33] have conducted numerous tests on bond stress τ_m, concluding that l_{cr} is proportional to d_{eq}/ρ_{eq}, as shown in Equation (5). On the basis of statistical analysis of extensive test data and considering engineering practice experience, the current design codes for concrete structures provide the calculation formula for average crack spacing, as shown in Equation (6). The comparison between the average crack spacing calculated by Equation (6) and the measured average crack spacing of the test slabs is presented in Table 7. The results show that the calculated values are much larger than the measured values, with the average value of l_{tcr}/l_{ccr} being 0.51. The calculation formula does not consider the influence of the high tensile strength of UHPC. Compared with ordinary concrete, UHPC has higher tensile strength and can bear greater tensile force between cracks. This makes the stress and strain of the longitudinal reinforcement between cracks more uniform, thereby affecting the crack spacing.

$$l_{cr} = K \cdot \frac{d_{eq}}{\rho_{ed}} \tag{5}$$

$$l_{cr} = \beta\left(1.9c + 0.08\frac{d_{eq}}{\rho_{te}}\right) \tag{6}$$

In the formula, k: test constant; β: coefficient related to the force-bearing state of the member, taking 1.0 for flexural members; and c: concrete cover thickness.

Table 7. Comparison between measured and calculated average crack spacing values of each test plate.

Specimen Number	l^t_{min}	l^t_{max}	l^t_{cr}	l^c_{cr}	l^t_{cr}/l^c_{cr}
XB-1	27	116	55.5	113.8	0.49
DB-1	29	124	57.6	113.8	0.51
DB-D	26	107	54.5	113.8	0.48
DB-3	22	101	53.1	92.7	0.57
DB-4	22	103	51.1	92.7	0.51
Average	——	——	——	——	0.51

Note, l^t_{min}: measured value of minimum crack spacing (mm); l^t_{max}: measured value of maximum crack spacing (mm); l^t_{cr}: measured value of average crack spacing (mm); l^c_{cr}: calculated value of average crack spacing (mm); ——: indicate none.

Due to the dense structure of UHPC and the incorporation of steel fibers, the bond strength between the UHPC and deformed reinforcement is significantly increased, which

reduces the relative slip between the concrete and reinforcement and minimizes the impact of bond-slip on crack spacing [34]. Considering that the concrete cover thickness of all test slabs is the same, the concrete cover thickness coefficient (1.9) remains unchanged. The bond-slip coefficient in the code calculation formula is modified. By performing linear regression on the variables d_{eq}/ρ_{te} and c using the measured average crack spacing l_{tcr}, the average crack spacing is obtained as shown in Equation (7). To verify the accuracy of the formula, the comparison between the calculation results of Equation (7) and the measured results of the test slabs is presented in Table 8. The results indicate that the calculated values from the modified formula and the measured values of the average crack spacing for each test slab have small dispersion, with little impact on the average crack spacing of the test slabs. The calculated values from the modified formula agree well with the measured values: the average value of l_{tcr}/l_{ccr} is 0.993, and the coefficient of variation is 0.024, indicating a low degree of data dispersion.

$$l_{cr} = 1.9c + 0.01\frac{d_{eq}}{\rho_{te}} \tag{7}$$

Table 8. Comparison between calculated and measured average crack spacing values.

Specimen Number	l_{cr}^{t} (mm)	l_{cr}^{t} (mm)	$l_{cr}^{t}/l_{cr}^{c\prime}$
XB-1	55.5	55.8	0.99
DB-1	57.6	55.8	1.03
DB-2	54.5	55.8	0.98
DB-3	53.1	53.2	1.00
DB-4	51.1	53.2	0.96
Average	——	——	0.993
Coefficient of variation	——	——	0.024

Note, ——: indicate none.

4.3. Maximum Crack Width Calculation

Due to the heterogeneity of concrete, crack spacing and crack width exhibit significant dispersion. In engineering verification, the primary concern is the maximum crack width. In this study, with reference to References [4,5], the calculation formula for the maximum crack width considering the characteristic combination of load effects and long-term load effects is as follows:

$$\omega_{\max} = \alpha_{cr}\psi\frac{\sigma_s}{E_s}l_{cr} \tag{8}$$

$$\psi = 1.1 - \frac{0.65f_{tk}}{\rho_{te}\sigma_s} \tag{9}$$

$$\sigma_s = \frac{M_q}{0.87A_sh_0} \tag{10}$$

In the formula, α_{cr}: coefficient of member force characteristic, taking 1.9 for flexural members; Ψ: coefficient of uneven strain of longitudinal tensile reinforcement between cracks, when $\psi < 0.2$, take $\psi = 0.2$ and when $\psi > 1.0$, take $\psi = 1.0$; Σ*s*: reinforcement stress at the cracked section under short-term load; *Es*: elastic modulus of reinforcement; *Mq*: bending moment value calculated according to the quasi-permanent combination of load effects; *As*: cross-sectional area of longitudinal reinforcement in the tensile zone; and h_0: effective cross-sectional height.

The comparison between the crack width ω_{cm} calculated by Equation (8) and the measured value ω_{tm} is presented in Table 9. It can be seen from Table 9 that under the cracking moment, the UHPC slabs can work normally with micro-fine cracks, whose width is usually less than 0.1 mm. Under the serviceability limit state, the measured values are slightly larger than the calculated values from the formula. This may be due to construction

and other factors: during the mixing and vibrating of concrete, steel fibers gradually settle to the bottom, resulting in more steel fibers in the lower part of the concrete instead of being uniformly dispersed in the UHPC. As a result, the bridging and crack-inhibiting effect of steel fibers is weakened. The average ratio of calculated values to measured values is 0.943, with a coefficient of variation of 0.038, indicating a low degree of data dispersion. It can be seen that the theoretical values agree well with the measured values. Therefore, the maximum crack width ω_{max} under short-term load can be calculated using the modified code formula.

Table 9. Comparison between calculated and measured crack width values.

Specimen Number	M_{cr}	M_k	$\omega^t{}_{m,cr}$	$\omega^t{}_{m,0.3}$	$\omega^c{}_{m,0.3}$	$\omega^t{}_{m,0.3}/\omega^c{}_{m,0.3}$
XB-1	7.395	30.03	0.039	0.265	0.30	0.883
DB-1	7.17	30.255	0.038	0.267	0.29	0.921
DB-2	6.99	35.16	0.037	0.311	0.32	0.972
DB-3	7.125	37.005	0.036	0.312	0.32	0.975
DB-4	7.025	36.695	0.035	0.309	0.32	0.966
Average	——	——	——	——	——	0.943
Coefficient of variation	——	——	——	——	——	0.038

Note, M_{cr}: mid-span cracking moment; M_k: mid-span bending moment at the serviceability limit state; $\omega^t{}_{m,cr}$: calculated crack width corresponding to the cracking moment; $\omega^t{}_{m,0.3}$: calculated crack width corresponding to the mid-span bending moment at the serviceability limit state; and $\omega^c{}_{m,0.3}$: recorded tested crack width at the serviceability limit state, ——: indicate none.

5. Conclusions

(1) UHPC composite slabs exhibit good plastic performance and belong to ductile failure. The cracking load of cast-in-place slabs is higher than that of UHPC composite slabs, but both the yield load and ultimate bearing capacity are lower. Compared with composite slabs without shear reinforcement and monolithic slabs, the performance of composite slabs equipped with stirrup stools and truss reinforcement is significantly improved. Among them, the yield load of truss-reinforced composite slabs is increased by 26.5%, and the ultimate load is increased by approximately 29.5–31%, which outperforms stirrup stool-reinforced slabs (yield load increased by about 18–19%, ultimate load increased by about 24–25%).

(2) During the flexural process of UHPC composite slabs, the section strain basically conforms to the plane section assumption, and the composite slabs maintain good integrity at all stages of bending. Shear key reinforcement can significantly improve the crack resistance and ductility of composite slabs. During the flexural process of UHPC composite slabs with stirrup stools and truss reinforcement, the cracks are characterized by high quantity, small width, small spacing, small length, and dense distribution. Truss reinforcement has a better effect on enhancing the crack resistance and ductility of composite slabs.

(3) Composite slabs with different loading methods have different cracking loads. However, after cracking, the crack-load curves are roughly parallel, and the crack development patterns are consistent.

(4) Based on the bond force transfer principle between reinforcement and concrete, a calculation formula for the average crack spacing is established. Considering the dense structure of UHPC and the contribution of steel fibers to bond strength, the bond-slip coefficient in the current code calculation formula is modified. The average crack spacing and the maximum crack width under the serviceability limit state are in good agreement with the test values.

Author Contributions: Conceptualization, C.L. and J.Z.; methodology, J.Z.; software, Y.L.; validation, Y.L., D.W. and J.Z.; formal analysis, Y.L.; investigation, J.Z.; resources, D.W.; data curation, C.L.;

writing—original draft preparation, C.L.; writing—review and editing, J.Z.; visualization, D.W.; supervision, Y.L.; project administration, J.Z.; funding acquisition, C.L. All authors have read and agreed to the published version of the manuscript.

Funding: The National Natural Science Foundation of China (No. 52178194); the Guangxi Science and Technology Program (No.AD25069101); The 2024 Project for Improving Scientific Research Basic Capabilities of Young and Middle-Aged Teachers in Guangxi Universities (No. 2024KY1763).

Data Availability Statement: The original contributions presented in this study are included in the article. Further inquiries can be directed to the corresponding authors.

Acknowledgments: This research was supported by the National Natural Science Foundation of China (Grant No. 52178194), the Guangxi Science and Technology Program (Project No.AD25069101), and the 2024 Project for Improving Scientific Research Basic Capabilities of Young and Middle-Aged Teachers in Guangxi Universities (Project No. 2024KY1763).

Conflicts of Interest: The authors declare no conflicts of interest.

References

1. De Larrard, F.; Sedran, T. Optimization of ultra-high-performance concrete by the use of a packing model. *Cem. Concr. Res.* **1994**, *24*, 997–1009. [CrossRef]
2. Rossi, P. Influence of fibre geometry and matrix maturity on the mechanical performance of ultra high-performance cement-based composites. *Cem. Concr. Compos.* **2013**, *37*, 246–248. [CrossRef]
3. Islam, R.U.; Khalil, J.; Hanif, A. Fatigue performance of ultra-high-performance concrete (UHPC): A critical review. *J. Build. Eng.* **2025**, *101*, 111881. [CrossRef]
4. Tang, J.; Feng, R.; Quach, W.; Zeng, J. Evaluation of flexural performance on corrosion-damaged RC beams retrofitted with UHPFRCC under marine exposure. *Eng. Struct.* **2025**, *333*, 114236. [CrossRef]
5. Jiang, H.; Li, J.; Gao, Y.; Zhang, L.; Fang, H.; Chen, Z.; Shi, Q. Shear strengthening of reinforced concrete (RC) beams using ultra-high performance concrete (UHPC) jacketing: Experimental analyses and calculation models. *J. Build. Eng.* **2026**, *118*, 114938. [CrossRef]
6. Yoo, S.-W.; Choi, Y.-C.; Choi, J.-H.; Choo, J.F. Nonlinear flexural analysis of composite beam with Inverted-T steel girder and UHPC slab considering partial interaction. *J. Build. Eng.* **2021**, *34*, 101887. [CrossRef]
7. Liu, Z.; Alsomiri, M.; Li, M.; Chen, X.; Meng, J. Experimental investigation on the flexural behavior of coarse aggregate reactive powder concrete (CA-RPC) bridge deck. *Eng. Struct.* **2022**, *271*, 114951. [CrossRef]
8. Lin, Y.; Yan, J.; Wang, Z.; Zou, C. Effects of steel fibers on failure mechanism of S-UHPC composite beams applied in the Arctic offshore structure. *Ocean. Eng.* **2021**, *234*, 109302. [CrossRef]
9. Zha, S.; Deng, W.; Liu, D.; Zhang, J.; Gu, J. Experimental study on flexural behavior of steel-laminated concrete (NC and UHPC) composite beams with corrugated steel webs. *Eng. Struct.* **2024**, *306*, 117802. [CrossRef]
10. Maj, M.; Ubysz, A. Cracking of composite fiber-reinforced concrete foundation slabs due to shrinkage. *Mater. Today Proc.* **2021**, *38*, 2092–2098. [CrossRef]
11. Liu, P.; Tang, P.; Feng, R.; Feng, R.; Xu, Y.; Zhu, J. Experimental investigation of the shear performance of corroded RC continuous beams strengthened with polarized CFRCM plates. *Eng. Struct.* **2025**, *333*, 120145. [CrossRef]
12. Wang, Z.; Yan, J.; Lin, Y.; Fan, F.; Yang, Y. Mechanical properties of steel-UHPC-steel slabs under concentrated loads considering composite action. *Eng. Struct.* **2020**, *222*, 111095. [CrossRef]
13. Luo, B.; Tang, Z.; Du, T.; Song, Y.; Cao, G. Experimental study on flexural performance of composite slab with UHPC layer. *Constr. Build. Mater.* **2025**, *492*, 143023. [CrossRef]
14. Chen, S.; Shi, X. Shear bond mechanism of composite slabs—A universal FE approach. *J. Constr. Steel Res.* **2011**, *67*, 1475–1484. [CrossRef]
15. Luo, B.; Tang, Z.; Zhao, F.; Song, Y.; Cao, G. Experimental investigation of the bending behavior of ribbed composite slabs with UHPC liner. *Case Stud. Constr. Mater.* **2025**, *23*, e05260. [CrossRef]
16. Zhang, Y.; Tan, C.; Zhao, H.; Tu, L.; Du, T.; Shao, X. Experimental and numerical study of shear-lag effect on low-ribbed steel-UHPC composite structure. *Structures* **2022**, *46*, 395–407. [CrossRef]
17. Al-Osta, M.A.; Isa, M.N.; Baluch, M.H.; Rahman, M.K. Flexural behavior of reinforced concrete beams strengthened with ultra-high performance fiber reinforced concrete. *Constr. Build. Mater.* **2017**, *134*, 279–296. [CrossRef]
18. Ren, Y.; Yang, Y.; Xu, P.; Liao, F. Mechanical mechanism and finite element analysis of laminated slab with split-joint under uniform load. *Build. Struct.* **2023**, *53*, 119–126. [CrossRef]

19. Thanoon, W.A.; Yardim, Y.; Jaafar, M.S.; Noorzaei, J. Structural behaviour of ferrocement–brick composite floor slab panel. *Constr. Build. Mater.* **2010**, *24*, 2224–2230. [CrossRef]
20. Luo, B. Influence of Constructional Pattern on Bending Stiffness of Composite Slab. *J. Hunan Univ. Sci.* **2023**, *50*, 36–44. [CrossRef]
21. Huang, W.; Luo, B.; Li, B.; Xu, X.; Su, Y. Experiment on Flexural Behavior of Green Concrete Composite Slab with Different Structural Forms. *J. Hunan Univ. Sci.* **2019**, *46*, 35–44.
22. Wu, H.; Qiao, G.; Qiao, Y.; Zhong, Z.; Zhou, Z.; Ye, T. Experimental and theoretical research on flexural performance of truss reinforced concrete two-way composite slab with prefabricated baseplate. *Structures* **2023**, *58*, 105470. [CrossRef]
23. Rahman, M.K.; Baluch, M.H.; Said, M.K.; Shazali, M.A. Flexural and Shear Strength of Prestressed Precast Hollow-Core Slabs. *Arab. J. Sci. Eng.* **2012**, *37*, 443–455. [CrossRef]
24. Zhao, Z.; Hu, Y.; Zhang, T. Experimental study on fire resistance of simple supported reinforced truss concrete laminated plates. *Build. Struct.* **2023**, *53*, 13–18. [CrossRef]
25. Fang, Z.; Fang, H.; Li, P.; Jiang, H.; Chen, G. Interfacial shear and flexural performances of steel–precast UHPC composite beams: Full-depth slabs with studs vs. demountable slabs with bolts. *Eng. Struct.* **2022**, *260*, 114230. [CrossRef]
26. Soliman, A.A.; Kumar, D.; Ranade, R.; Heard, W.F.; Williams, B.A. Review of flexural behavior and design recommendations for ultra-high performance concrete members. *Structures* **2024**, *62*, 106237. [CrossRef]
27. Cao, X.; Li, Y.; Liu, C. Experimental study on flexural behavior of UHPC composite slab with the steel of combined interface. *Concrete* **2022**, *09*, 1–5.
28. Kalateh, F.; Ojaghi, K.; Yaghin, M.A.L. Experimental and numerical study on the pull-out behavior of steel fibers in ultra-high-strength concrete reinforced with biodegradable nanoparticles. *Constr. Build. Mater.* **2025**, *500*, 144171. [CrossRef]
29. Zhang, J.; Tang, W.; Yi, J.; Huang, D.; Wang, L.; Qin, Q. A review of coral aggregate concrete and FRP-reinforced coral aggregate concrete: From materials characterization to structural applications. *Structures* **2025**, *82*, 110617. [CrossRef]
30. Zhang, J.; Wang, L.; Yi, J.; Qin, Q. Experimental study on stress-strain relationship of high strength coral concrete (HSCC). *J. Build. Eng.* **2024**, *87*, 109090. [CrossRef]
31. Lou, C.; Su, J.; Zhao, X.; Wu, D.; Ma, J.; Li, Z.-X. Eccentric pull-out test and numerical investigation of bond behavior of corroded high-strength steel bars in ultra-high performance steel fiber-reinforced concrete (UHPSFRC). *Eng. Struct.* **2025**, *342*, 120932. [CrossRef]
32. Oliveira, R.S.; Ramalho, M.A.; Corrêa, M.R.S. A layered finite element for reinforced concrete beams with bond–slip effects. *Cem. Concr. Compos.* **2008**, *30*, 245–252. [CrossRef]
33. Galkovski, T.; Mata-Falcón, J.; Kaufmann, W. Stress field model for bond in reinforced concrete ties. *Eng. Struct.* **2023**, *294*, 116759. [CrossRef]
34. Aiamsri, K.; Yaowarat, T.; Horpibulsuk, S.; Suddeepong, A.; Buritatum, A.; Hiranwatthana, K.; Nitichote, K. Bonding behavior of lap-spliced reinforcing bars embedded in ultra-high-performance concrete with steel fibers. *Dev. Built Environ.* **2024**, *20*, 100585. [CrossRef]

Disclaimer/Publisher's Note: The statements, opinions and data contained in all publications are solely those of the individual author(s) and contributor(s) and not of MDPI and/or the editor(s). MDPI and/or the editor(s) disclaim responsibility for any injury to people or property resulting from any ideas, methods, instructions or products referred to in the content.